Monthly Notices
of the
ROYAL ASTRONOMICAL SOCIETY

Mon. Not. R. Astron. Soc. **400,** 1726–1733 (2009) doi:10.1111/j.1365-2966.2009.15585.x

CO observations towards bright-rimmed clouds

L. K. Morgan,[1⋆] J. S. Urquhart[2] and M. A. Thompson[3]

[1] *St Mary's University, 923 Robie Street, Halifax, Nova Scotia B3H 3C3, Canada*
[2] *Australia Telescope National Facility, CSIRO, Sydney, NSW 2052, Australia*
[3] *Centre for Astrophysics Research, Science and Technology Research Institute, University of Hertfordshire, College Lane, Hatfield AL10 9AB*

Accepted 2009 August 20. Received 2009 August 19; in original form 2009 June 22

ABSTRACT

Bright-rimmed clouds (BRCs) appear to be sites of triggered star formation induced through the propagation of shocks initiated by the expansion of nearby H II regions. Our main aim is to establish support for observations of star-forming activity within a sample of BRCs. A secondary aim is to establish a plausible link between such star formation and observed external influences. We have conducted CO (J = 2–1) observations using the James Clerk Maxwell Telescope to probe the environments of a sample of star-forming BRCs associated with embedded protostellar cores. Local thermodynamic equilibrium analysis allows the determination of the physical properties of these protostars and investigation of the structure and kinematic motions within the molecular gas. Using a combination of archival radio and mid-infrared data, and submillimeter observations, we have refined the Sugitani, Fukui and Ogura (SFO) catalogue, excluding 18 BRCs that do not show any evidence of photoionization induced collapse. Of the remaining 26 clouds that are being photoionized, we find 20 that are associated with embedded protostars. These 20 clouds are excellent candidates with which to further investigate the radiatively driven implosion mode of triggered star formation. Comparing the physical parameters of the triggered and untriggered samples, we find that the surface temperatures of the potentially triggered clouds are significantly higher (by ∼10 K) than those in which triggering is considered unlikely. The higher surface temperatures found towards the sample of potentially triggered clouds are consistent with the hypothesis that these clouds are being externally heated through their exposure to the H II region.

Key words: line: profiles – stars: formation – ISM: Clouds – H II regions.

1 INTRODUCTION

High mass stars can influence subsequent local star formation through the propagation of shocks into the surrounding molecular material that can compress the gas and lead to the formation of dense cores, which can subsequently collapse to form a new generation of stars. This mode of *triggered* star formation is known as radiatively driven implosion (RDI).

Individual high-mass stars (or clusters of the same) rapidly ionize the material surrounding them shortly after they begin core hydrogen burning. The ionized 'bubble' surrounding the new massive star expands on a short time-scale until it reaches the Strömgren radius at which the ionizing flux of the driving star is matched by the recombinations occurring within the interstellar material. At this point, molecular clouds exterior to the H II region begin to feel the effects of the highly luminous ionizing sources within the H II region. At the border of the H II region, the photoionizing photons will develop an ionized boundary layer (IBL), provided that molecular material exists there with a density sufficiently high to support it. This IBL is a dense shell of ionized gas on the exterior of the molecular cloud, the material within will flow radially away from the molecular cloud into the relatively low pressure of the recently formed H II region.

The relatively high densities within the IBLs lead to higher recombination rates which shield the cloud from quickly evaporating (Reipurth 1983). The increased pressure due to ionization heating in the ionized gas causes an expansion of the IBL into the intercloud medium and an ionization front preceded by a shock in the neutral gas propagates into the cloud (Lefloch & Lazareff 1994; White et al. 1997). According to theories and models of RDI (e.g. Bertoldi 1989; Lefloch & Lazareff 1994; Miao et al. 2006; Gritschneder et al. 2009; Miao et al. 2009), these shocks may trigger the formation and/or collapse of dense, otherwise quiescent, clumps within the clouds.

Bright-rimmed clouds (BRCs) are isolated molecular clouds located on the peripheries of evolved H II regions. Their optically bright rims are a result of recombination within the IBLs. Many BRCs display a cometary morphology, i.e. a collimated structure or curved edge. These clouds invariably align with the long axis of the column parallel to the direction of an ionizing source, for example a

⋆E-mail: lmorgan@ap.smu.ca

© 2009 The Authors. Journal compilation © 2009 RAS

nearby OB star. Their isolation and simple morphology make these clouds ideal environments with which we investigate the RDI mode of star formation.

In an effort to investigate the RDI mode of star formation, Sugitani and collaborators (Sugitani, Fukui & Ogura 1991; Sugitani & Ogura 1994) searched the Sharpless H II region catalogue (Sharpless 1959) and the European Southern Observatory (Red) [ESO(R)] Southern Hemisphere Atlas for clouds located on the peripheries of H II regions with optically bright rims. They cross-matched these with far-infrared (far-IR) point sources from the *IRAS* point source catalogue which had colours indicative of embedded protostars. The search resulted in the identification of 89 BRCs, 44 located in the northern hemisphere and 45 located in the southern hemisphere; these are collectively known as the SFO catalogue. A number of these clouds show evidence for a spatiotemporal age gradient with older stars found closer towards the ionizing stars of the H II regions and younger (T Tauri) stars found progressively nearer the rims of the BRCs (e.g. Getman et al. 2007; Ikeda et al. 2008; Chauhan et al. 2009; Getman et al. 2009), which is consistent with RDI and the small-scale sequential star formation hypothesis.

These BRCs are possible examples of triggered star formation, in which photoionization driven shocks propagate into clouds of dust and gas at the boundary of ionized regions. We are conducting a multiwavelength programme of observations in order to provide a complete census of the embedded star formation within these clouds. This will allow us to fully evaluate the efficiency of this mode of star formation. In previous papers, we have presented radio continuum observations and mid-IR imaging towards the whole SFO catalogue (Thompson, Urquhart & White 2004; Morgan et al. 2004, hereafter Paper I). In addition, submillimetre (submm) maps of dust emission associated with the clouds (Morgan et al. 2008; hereafter Paper II) and CO observations (Urquhart, Morgan & Thompson 2009) have been made towards northern and southern samples, respectively. We have also conducted some detailed studies of individual clouds and small subsamples (Thompson et al. 2004; Thompson & White 2004; Urquhart et al. 2004, 2006, 2007).

In this paper, we present CO spectra towards a sample of northern BRCs which were found to be associated with high column densities of dust. These observations allow us to begin to characterize the properties of the molecular gas, and are a first step in probing the kinematics and structure of these clouds. Using the results of our previous observations towards the northern BRCs, we refine the initial sample, eliminating clouds where the star formation is unlikely to have been triggered, and compare the CO properties of the triggered and untriggered samples. In the next section, we describe our observations and data reduction. In Section 3, we present our results and analysis; the significance of these is discussed in Section 4. In Section 5, we present a summary of our results and highlight our main findings.

2 OBSERVATIONS AND DATA REDUCTION

Observations of the CO (J = 2–1) transition were made using the James Clerk Maxwell Telescope (JCMT). Sources were selected from the examination of Submillimetre Common-User Bolometer Array (SCUBA) maps of each source from previous observations (Paper II). We attempted to prioritize sources identified as being good triggered candidates. However, these observations were executed in the queue-based observing system and so were chosen as weather and hour angle allowed. As a result, the presented sample contains both candidate triggered and untriggered sources.

Observations presented in this paper were made using Receiver A3 on the JCMT. The majority of our observations were taken between 2004 February and July using the Digital Autocorrelation Spectrometer (DAS) as the back end. Repeat position-switched observations of SFO 1, 2 and 3 in the ^{13}CO and C^{18}O lines were carried out in 2008 October using the new Auto-Correlation Spectrometer and Imaging System (ACSIS) back end as the 2004 DAS data were found to be corrupted. Single pointed observations were made, using frequency switching for sky removal, of all spectral lines presented here apart from ^{12}CO. Position switching was used for the ^{12}CO observations as this transition is expected to have large linewidths (possibly greater than the frequency throw of the DAS). The DAS spectra possess a bandwidth of 160 MHz with 2048 channels and corresponding channel spacing of 78 kHz and a spectral resolution of 94 kHz. The ACSIS spectra of SFO 1, SFO 2 and SFO 3 possess a 250 MHz bandwidth with 8196 channels and a corresponding channel spacing of 30.5 kHz. As frequency switching had not yet been commissioned for ACSIS, these spectra were obtained in position-switched mode. All spectra were calibrated using the standard chopper wheel technique to place them on the $T_{\rm A}^{*}$ scale (e.g. Kutner & Ulich 1981). Typical observed rms levels were 0.2, 0.1 and 0.1 K for typical integration times of 2, 10 and 20 m for the ^{12}CO, ^{13}CO and C^{18}O transitions, respectively. The full width at half-maximum beam size of the JCMT is ∼22 arcsec at 230 GHz.

In total, observations were made towards 19 BRCs; however, a separate observation was made towards each of the two dust cores detected within SFO 25 (Paper II, referred to here as SFO 25a and SFO 25b), which brings the total number of sources observed to 20. The pointing positions for each observation were determined from the peak emission positions taken from the 850 μm SCUBA maps presented in Paper II. In a few cases, this position was not well determined at the time and, for SFO 24, SFO 27 and SFO 33, subsequently revised. In Table 1, we present a summary of the BRCs observed and the pointing centres used for the observations.

Data were reduced in the standard manner using the STARLINK package SPECX (Prestage et al. 2000) and baselines removed through polynomial baseline subtraction. Spectral line profiles were fit using

Table 1. Sources observed and pointing positions.

Catalogue Id.	RA (J2000)	Dec. (J2000)
SFO 01	23:59:32.3	+67:24:03
SFO 02	00:03:58.6	+68:35:12
SFO 03	00:05:22.7	+67:17:56
SFO 05	02:29:01.7	+61:33:32
SFO 07	02:34:48.1	+61:46:35
SFO 09	02:36:27.7	+61:24:01
SFO 10	02:48:12.4	+60:24:34
SFO 15	05:23:28.3	+33:11:48
SFO 16	05:19:48.2	−05:52:04
SFO 18	05:44:29.9	+09:08:56
SFO 23	06:22:58.3	+23:10:12
SFO 24	06:34:52.7	+04:25:23
SFO 25a	06:41:03.3	+10:15:09
SFO 25b	06:41:04.7	+10:14:59
SFO 27	07:04:00.5	−11:22:58
SFO 30	18:18:46.7	−13:44:27
SFO 31	20:50:43.1	+44:21:57
SFO 33	21:33:13.8	+57:30:04
SFO 34	21:33:32.2	+58:03:34
SFO 36	21:36:07.1	+57:26:42

the Onsala Space Observatory spectral line analysis package xs.[1] Generally, Gaussian fitting was achieved through best-fitting methods of the parameters of linewidth, peak height and central velocity. In the case of self-absorption or shoulder or wing emission, one or more of these parameters may have been fixed; this was determined on a source-by-source basis.

3 RESULTS

A total of 20 sources have been observed with CO emission being detected towards every source. Due to observational constraints, only the ^{13}CO transition was observed towards every source, with observations of the ^{12}CO and C^{18}O transitions being made towards 17 and 18 sources, respectively. All sources observed in ^{12}CO and ^{13}CO were detected, with two non-detections in C^{18}O (SFO 10 and 15). In Fig. 1, we present plots of the emission lines detected, overplotted with the Gaussian fits to these data. The emission seen in the ^{12}CO transition towards SFO 18 and SFO 31 is too complex to be well fit by a Gaussian and therefore no fits have been overplotted. In Table 2, we present the physical parameters determined from the Gaussian fit to the spectra. In this table, sources not observed in a particular transition are indicated by dashes, as are the entries for the ^{12}CO transitions for SFO 18 and SFO 31.

As can be seen in Fig. 1, in the majority of cases a simple Gaussian profile provides a good fit to the data (particularly for the ^{13}CO and C^{18}O transitions); however, in a significant number of our sources the emission profile can be seen to deviate significantly from the Gaussian profile. These non-Gaussian profiles, which are most obvious in the optically thick ^{12}CO transition, can be classified into several distinct types: wings; shoulder; flat top and self-absorption. These features are interesting in themselves since they can give an indication of dynamic motions within the gas. For example, non-Gaussian line 'wings' are often found to be associated with molecular outflows (Wu et al. 2004), shoulders and asymmetric profiles can indicate shocked motions within the gas (as might be expected if a cloud is undergoing RDI; Elmegreen & Moran 1979), and asymmetric self-absorption features can be produced by infall motions (Myers et al. 1996) [though it should be noted that De Vries, Narayanan & Snell (2002) found that BRCs may actually be less likely to exhibit infall signatures than other star-forming regions]. It is not possible to unequivocally attribute these profiles to any particular origin from a single spectrum. However, the presence of these non-Gaussian profiles is a good indication that these clouds are dynamically interesting and we therefore note their presence in the final column of Table 2 along with previously detected outflow activity, revealed in a literature search of our source list.

From inspection of the profiles, we find eight clouds that are associated with line wings (40 per cent of the sample). One cloud shows a likely self-absorbed profile, two clouds appear saturated (flat-topped) and a further two clouds appear either saturated, self-absorbed or a combination of the two. In total, 13 of the 20 sources observed display some type of non-Gaussian profile (65 per cent of the sample). Taking into account the lack of ^{12}CO data for three sources, in which these features are most prominent, a corresponding proportion of 75 per cent may be more accurate. The submm observations of Paper II identified embedded protostars within the majority of the clouds observed. The detection of non-Gaussian profiles towards a large fraction of these is further confirmation that star formation is currently taking place within them.

3.1 CO observational analysis

The corrected antenna temperatures of each of the three CO species observed are presented in Table 2 along with linewidths and local standard of rest (LSR) velocities. It may be expected that emission of ^{12}CO is optically thick in these clouds. The small ratio of line intensities of ^{12}CO to ^{13}CO ($\overline{I_{12}/I_{13}} \sim 4$) supports this, given that the expected abundance ratio of these isotopes is $\sim$70 in Photon Dominated Regions (PDRs) (Savage et al. 2002). Thus, the excitation temperature of the ^{12}CO (J = 2–1) transition may be determined from the equation

$$T_{\rm ex} = 11.06 \left[\ln \left(1 + \frac{11.06}{T_{\rm B} + 0.196} \right) \right]^{-1}, \quad (1)$$

where $T_{\rm B}$ is the brightness temperature of the ^{12}CO line, derived assuming a forward spillover efficiency for the JCMT at these frequencies[2] of 0.8. It is also assumed that the coupling efficiency of the sources to the beam is unity as the sources are extended on the scale of the beamwidth ($\sim$22 arcsec at 230 GHz).

It is likely that there may be significant differences between the temperature measured at the optical depth of ^{12}CO and that measured by the ^{13}CO and C^{18}O lines. The exterior regions of the clouds are preferentially probed by the ^{12}CO line due to the opacity of the transition. These regions are likely to be higher in temperature than the interior regions due to heating from the interstellar radiation field and the predicted flux from nearby massive stars. The heads of the clouds are also often centrally condensed (Paper II) and so the interiors may be expected to be cooler through more efficient radiation transport.

For these reasons, we have independently calculated the opacity of C^{18}O using the ratio of line temperatures $T_{^{13}\rm CO}/T_{\rm C^{18}O}$, assuming that the optically thin limit applies for C^{18}O and that ^{13}CO emission is at most moderately optically thick ($\tau \lesssim 1$). In this case, we may use the relation

$$\frac{T_{13}}{T_{18}} = \frac{1 - {\rm e}^{\tau_{13}}}{1 - {\rm e}^{\tau_{18}}}, \quad (2)$$

where T_{13} and T_{18} are the corrected antenna temperatures and τ_{13} and τ_{18} are the optical depths of the ^{13}CO and C^{18}O transitions, respectively. By assuming a ratio of $\chi^{13}_{18} = 10$ for the abundance of ^{13}CO with relation to C^{18}O (e.g. Urquhart et al. 2006), we may solve for optical depth via $\tau_{13} = \chi^{13}_{18}\,\tau_{18}$. Knowing the optical depth of the C^{18}O transition, we may then find its excitation temperature through

$$T_{\rm ex} = 10.54 \left\{ \ln \left[1 + \frac{10.54(1 - {\rm e}^{-\tau})}{T_{\rm B} + 0.227(1 - {\rm e}^{-\tau})} \right] \right\}^{-1}. \quad (3)$$

Given the excitation temperature of C^{18}O (J = 2–1), one may determine the column density of that species (in all transitions) through the equation

$$N_{\rm Tot} = \frac{1.87 \times 10^9 T_{\rm ex}^2 {\rm e}^{\frac{5.27}{T_{\rm ex}}} \int T_{\rm B} {\rm d}v}{\left(\frac{1}{{\rm e}^{10.54/T_{\rm ex}} - 1} - \frac{1}{{\rm e}^{10.54/T_{\rm bg}} - 1} \right)} \ {\rm cm}^{-2}. \quad (4)$$

[1] For more details see http://www.chalmers.se/rss/oso-en/observations/data-reduction-software.

[2] Guide to spectral line observing at the JCMT. H. E. Matthews, J. Leech, P. Friberg.

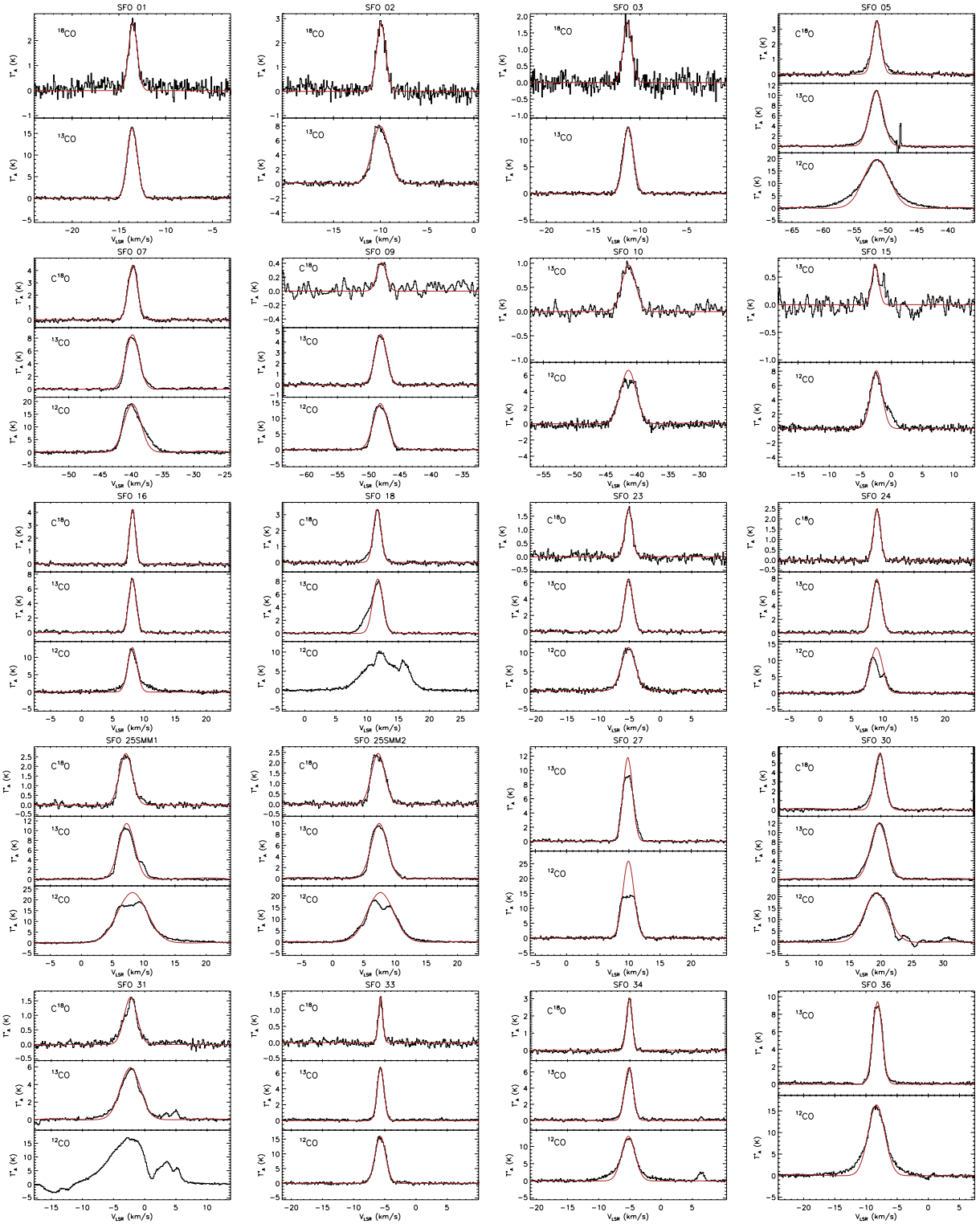

Figure 1. Spectral lines are presented with corrected antenna temperature, T_A^*, plotted against Doppler shifted velocity, V_{LSR}. Multiple lines are plotted on the same axes with individual species labelled. Gaussian fits to spectra are overlaid in red.

By taking the value of the fractional abundance of $C^{18}O$ as compared to H_2 as 1.7×10^{-7} (Goldsmith, Bergin & Lis 1996), H_2 column densities for the observed clouds may be calculated. We present these column densities along with the internal and external excitation temperatures and the $C^{18}O$ optical depths in Table 3.

4 DISCUSSION

In this section, we will discuss the CO observations in conjunction with the results obtained from our IR, submm and radio analyses presented in Papers I and II. Combining all of these data sets allows

© 2009 The Authors. Journal compilation © 2009 RAS, MNRAS **400,** 1726–1733

Table 2. CO spectra fitted parameters.

Catalogue Id.	^{12}CO T_A^* (K)	^{12}CO dV (km s^{-1})	^{12}CO V_{LSR} (km s^{-1})	^{13}CO T_A^* (K)	^{13}CO dV (km s^{-1})	^{13}CO V_{LSR} (km s^{-1})	C^{18}O T_A^* (K)	C^{18}O dV (km s^{-1})	C^{18}O V_{LSR} (km s^{-1})	Profile Notes and References[a]
SFO 01	–	–	–	16.4	1.3	−13.6	2.7	1.1	−13.5	
SFO 02	–	–	–	8.0	2.1	−10.0	2.8	1.2	−9.9	
SFO 03	–	–	–	12.5	1.3	−11.2	1.8	1.1	−11.3	
SFO 05	19.7	4.9	−51.4	10.9	2.6	−51.5	3.6	1.6	−51.4	Wings [1]
SFO 07	19.1	3.2	−39.8	8.5	2.5	−39.8	4.4	1.8	−39.7	Blue wing [2]
SFO 09	14.8	2.7	−48.1	4.7	2.2	−48.1	0.4	1.8	−47.9	
SFO 10	6.6	3.0	−41.4	1.0	2.6	−41.31	<0.3			Saturated
SFO 15	8.1	2.2	−2.4	0.7	1.3	−2.6	<0.3			
SFO 16	12.8	1.8	8.1	7.3	1.4	8.1	4.2	1.1	8.2	Wings [3]
SFO 18	–	–	–	8.3	1.9	11.7	3.3	1.5	11.6	Red wing/shoulder [4]
SFO 23	11.4	2.6	−5.2	6.5	1.6	−5.1	1.8	1.4	−5.1	
SFO 24	13.9	2.3	9.0	7.9	1.7	9.0	2.5	1.3	9.1	Self-absorption
SFO 25a	23.4	5.6	8.2	11.5	3.0	7.2	2.7	2.4	7.1	Self-absorption/saturated [5]
SFO 25b	21.5	5.0	7.6	10.0	3.0	7.4	2.5	2.5	7.3	Self-absorption/saturated [5]
SFO 27	25.8	2.1	9.9	9.8	1.8	11.8	–	–	–	Saturated
SFO 30	21.9	4.5	19.3	11.9	3.1	19.7	6.0	2.0	19.8	Red wing
SFO 31	–	–	–	5.9	3.8	−2.3	1.6	2.4	−2.3	Red wing
SFO 33	15.9	2.0	−5.7	6.7	1.3	−5.7	1.4	0.8	−5.7	
SFO 34	12.9	2.6	−5.2	6.6	1.6	−5.2	3.1	1.1	−5.1	Wings
SFO 36	16.4	3.2	−8.3	9.4	1.8	−8.2	–	–	–	Wings

Notes: – indicates that a source was not observed in this transition or, in the cases of SFO 18 and SFO 31, that the ^{12}CO spectra is too complex to be reliably represented by a Gaussian fit to the data.

[a]Outflow activity previously detected by [1] Fukui et al. (1993), Lefloch, Lazareff & Castets (1997), Wu et al. (2004); [2] Wu et al. (2004); [3] Fukui et al. (1993), De Vries et al. (2002), Wu et al. (2004), Beltrán et al. (2008); [4] De Vries et al. (2002), Wu et al. (2004); [5] De Vries et al. (2002).

Table 3. Physical quantities derived from the CO data.

Catalogue Id.	T_{ex} (^{12}CO) (K)	T_{ex} (C^{18} O) (K)	τ (C^{18} O)	$\log_{10}$(N(H$_2$)) (cm^{-2})
SFO 01	–	33.7	0.12	21.73
SFO 02	–	14.8	0.42	21.96
SFO 03	–	28.4	0.10	21.56
SFO 05	30.0	18.9	0.39	22.13
SFO 07	29.3	15.5	0.73	22.32
SFO 09	23.8	–	–	–
SFO 10	13.2	–	–	–
SFO 15	15.2	–	–	–
SFO 16	21.2	13.9	0.86	22.13
SFO 18	18.0[a]	15.4	0.50	22.12
SFO 23	19.5	13.2	0.31	21.87
SFO 24	22.7	15.0	0.37	21.94
SFO 25a	34.7	20.9	0.24	22.16
SFO 25b	32.3	18.6	0.26	22.17
SFO 27	37.7	–	–	–
SFO 30	32.8	19.9	0.70	22.43
SFO 31	26.6[a]	12.5	0.30	22.09
SFO 33	25.2	14.5	0.20	21.50
SFO 34	21.4	13.1	0.63	22.02
SFO 36	25.8	–	–	–

[a]No Gaussian profile was fit to the ^{12}CO line of these sources, the peak line temperature measured was therefore used to determine T_{ex} for ^{12}CO.

us to refine the original sample of BRCs by eliminating the more diffuse clouds, and thus properly interpret the CO results in the context of the triggered star formation scenario.

4.1 Refining the SFO catalogue

In Paper I, we presented archival radio continuum images obtained from the NRAO (National Radio Astronomy Observatory) VLA (Very Large Array) Sky Survey (NVSS) (Condon et al. 1998; 20 cm) and Midcourse Space Experiment (MSX) mid-IR images for the whole northern sample. The radio continuum data trace any ionized gas associated with these BRCs, which we would expect to find in a layer between the front of the clouds and the H II region – this region is commonly referred to as the IBL mentioned in the introduction. The presence of an IBL is an excellent indication that there is a strong interaction between the H II region and the molecular cloud. In addition to the IBLs, the mid-IR images reveal the presence of strong 8 μm emission along the exposed edge of these clouds. The MSX 8 μm filter is dominated by emission from polycyclic aromatic hydrocarbons (PAHs). These molecules absorb radiation at far-ultraviolet wavelengths and re-emit the energy in the IR regime (Leger & Puget 1984). Notable spectral features of these molecules are found at 7.7 and 8.6 μm which are traced by the MSX 8 μm filter. These images are, therefore, a good tracer of the photon-dominated region, which is a layer between the ionization front and the neutral molecular region of the clouds.

The analysis performed in Paper I allows us to establish the triggered status of the BRCs of the SFO catalogue, or at least to refine our sample to eliminate sources that are highly unlikely to have been triggered. Our main criterion for establishing triggered status is identification of an IBL associated with the edge of each BRC. The lack of a detectable IBL in any given BRC would make a triggered formation scenario unlikely (at least in the context of the RDI scenario). The detection of an IBL in 20-cm free–free emission is therefore considered to be evidence of *potential* triggering through

the RDI process, supported by the detection of 8.3 μm emission as reported in Paper I.

The combination of radio and mid-IR data allows us to identify 25 BRCs that show strong evidence of a significant interaction with their host H II regions; these are considered excellent candidates in which observed star formation may have been triggered.

The source SFO 14 merits special mention, this source was not identified as a likely triggered candidate in Paper I as the radio emission emanating from the cloud's rim is not associated with MSX emission. The cloud is host to a well-studied Ultra Compact HII (UCHII) region (see Paper I) which dominates the local mid-IR emission. It is possible that the UCHII region may mask IR emission associated with the cloud's rim and, in addition, there are several recent studies which appear to indicate that, while the UCHII region itself is of uncertain origin, Class I and II sources associated with the cloud as a whole show properties consistent with formation resulting from interaction with the exciting ionizing star (Matsuyanagi et al. 2006; Koenig et al. 2008). Therefore, this source is included in our sample of potentially triggered regions.

We are able to eliminate 18 clouds towards which no radio emission has been detected and the evolution of which is unlikely to be significantly affected by the nearby OB star(s). The 26 BRCs which we have determined are candidates for triggered star formation are listed explicitly in Table 4.

Our analysis of the radio continuum and mid-IR archival data was followed up by submm observations of the majority of the clouds in the northern sample using SCUBA (i.e. Paper II). The aim of these submm observations was to map the distribution of dust towards the BRCs and to identify any protostars embedded within them. In total, 38 of the 44 northern sample of BRCs were observed, including all of the 26 potentially triggered BRCs listed in Table 4. Submm emission from warm dust was detected towards 25 of these clouds (no emission was detected towards SFO 6). The distribution of dust for a large fraction of these potentially triggered clouds appears to be centrally condensed, and the analysis of the spectral energy distribution of these sources indicates that the cores are likely to host embedded protostars in the earliest stages of their evolution (see Paper II for more details).

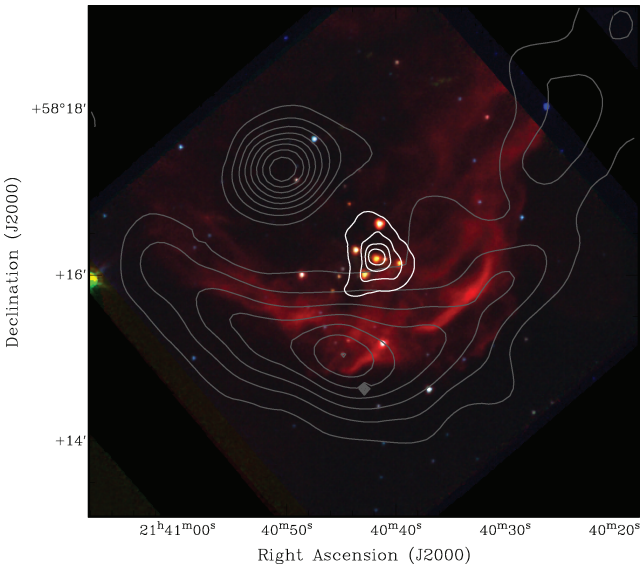

Figure 2. The colour composite *Spitzer* image of SFO 38 constructed using the 3.6, 4.5 and 8.0 μm filter of IRAC shown in blue, green and red, respectively. We overlay contours of the NVSS radio emission (grey) and the submm emission at 850 μm from dust (white). Both sets of contours begin at a level of three times the rms noise of their respective images, then increase in increments of 20 per cent of the relative peak fluxes.

As an example of a source exhibiting likely triggered star formation, in Fig. 2 we present a composite image of SFO 38. The image presented in this figure is constructed from the 3.6 (blue), 4.5 (green) and 8.0 (red) μm filters of the Infrared Array Camera (IRAC) on the *Spitzer Space Telescope*. The 8.0 μm filter is dominated by PAH emission which is excited by UV photons from the H II regions and so traces the cloud's rim. We have overlaid contours of the radio (grey) and submm (white) emission to illustrate the morphological correlation between the ionized gas, the cloud's rim and the location of the embedded protostar. This image illustrates the morphological correlation between the IBL traced by the radio emission and the photon-dominated region within the surface layers of the cloud. A second radio source is seen located behind the clouds rim, away from the direction of the ionizing star. However, this is not correlated with any mid-IR structure within the cloud and is therefore likely to be the result of a chance alignment with an extragalactic background source. The SCUBA data reveal the presence of a dense core located just beyond the cloud's rim, with respect to the direction of the ionizing source, consistent with the location predicted by RDI models (Lefloch & Lazareff 1994; Miao et al. 2006). Furthermore, inspection of the image reveals the presence of five embedded sources, all of which are located with the

Table 4. Star-forming regions likely to have been triggered.

Catalogue Id.	RA (J2000)	Dec. (J2000)	Luminosity[a] ($L_\odot$)	Dist. (kpc)	Rim Type
SFO 01	23:59:32.3	+67:24:03	122	0.85	B
SFO 02	00:03:58.6	+68:35:12	57	0.85	A
SFO 04	00:59:01.0	+60:53:29	1	0.19	B
SFO 05	02:29:02.2	+61:33:33	1154	1.90	B
SFO 06	02:34:45.1	+60:47:48	160[b]	1.90	A
SFO 07	02:34:47.8	+61:46:29	400	1.90	B
SFO 10	02:48:12.3	+60:24:32	268	1.90	A
SFO 11[c]	02:51:33.7	+60:03:54	330	1.90	A
SFO 12	02:55:01.5	+60:35:43	201	1.90	B
SFO 13	03:00:56.5	+60:40:24	444	1.90	B
SFO 14	03:01:31.3	+60:29:20	3205	1.90	A
SFO 15	05:23:28.3	+33:11:48	317	3.40	B
SFO 25	06:41:04.0	+10:15:05	43	0.78	B
SFO 27	07:03:58.3	−11:23:04	108	1.15	A
SFO 30	18:18:46.8	−13:44:28	6945	2.20	B
SFO 31	20:50:43.1	+44:21:56	96	1.00	A
SFO 32	21:32:29.5	+57:24:33	43[b]	0.75	A
SFO 35	21:36:03.4	+58:31:25	<13[b]	0.75	A
SFO 36	21:36:07.4	+57:26:41	110[b]	0.75	A
SFO 37	21:40:28.9	+56:35:53	63	0.75	C
SFO 38	21:40:41.8	+58:16:14	340[b]	0.75	B
SFO 40	21:46:13.4	+57:09:42	16	0.75	A
SFO 41	21:46:28.6	+57:18:35	15	0.75	B
SFO 42	21:46:34.7	+57:12:31	16	0.75	A
SFO 43	22:47:49.3	+58:02:51	1385	2.40	B
SFO 44	22:28:51.1	+64:13:40	1000[b]	0.91	A

[a]Sources luminosities indicated by [b] are determined from *IRAS* observations, as reported by Sugitani et al. (1991). The luminosity of SFO 11 relates to the source SFO 11 SMM1 as reported by Thompson et al. (2004). All other source luminosities are taken from Paper II.

[c]Position and luminosity is that of SFO 11 SMM1, taken from Thompson et al. (2004).

boundary of the dust core with one source being coincident with the peak of the dust emission.

Using a combination of archival radio and mid-IR data, and submm observations as described above, we have refined the SFO catalogue. We find that only ∼59 per cent of the original sample appears likely to have been triggered, having eliminated 18 BRCs that do not show any evidence of photoionization. These proportions are similar to those found towards the southern sample of BRCs (Sugitani & Ogura 1994) recently reported by Urquhart et al. (2009).

4.2 Interpreting the CO results

At the beginning of this section, we separated the northern SFO sample into two distinct groups which can be classified as (I) potentially triggered star-forming regions and (II) protostellar clouds unlikely to have been triggered. Since our CO observations were made whilst the analyses of the radio and submm data were still at an early stage, and therefore without prior knowledge of these classifications, they have effectively sampled both groups. The only condition set on the CO observations was that submm emission was detected towards the observed sources, and this therefore biases the observations towards dense star-forming clouds.

Of the 20 sources observed with the JCMT, 12 are in group I, leaving eight in group II. As the sample is approximately equally divided between potentially triggered and non-triggered sources, we are in a position to compare their physical parameters in an effort to identify any differences that exist.

In Table 3, we present a summary of the derived physical parameters obtained from the CO data. Comparing the internal temperatures, opacities and densities of the two groups, we find no significant differences – this is somewhat to be expected since star formation is likely to be ongoing within the majority of clouds observed. However, we do find a difference in the external temperatures between the potentially triggered (group I) and untriggered (group II) samples. In Fig. 3, we present a histogram plot of the ^{12}CO excitation temperatures of the potentially triggered sources and the untriggered sources. This plot shows that the clouds that have been identified as triggered have a significantly higher external temperature than those considered unlikely to have been triggered. Typical external temperatures for the triggered and untriggered groups are ∼30–35 and 20–25 K, respectively (median averages are 30 and 21 K). A Kolmogorov–Smirnov test of the temperature distributions of the two samples rejects the null hypothesis that the samples are drawn from the same population with a confidence of 97 per cent. The higher external temperatures found towards the triggered sample are consistent with the fact that their surface layers are being externally heated by radiation from the nearby OB stars.

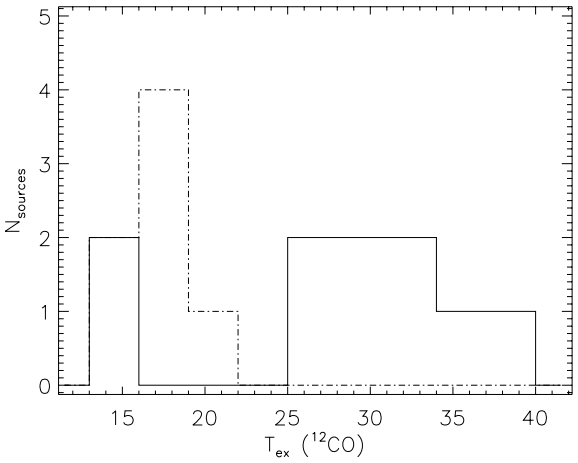

Figure 3. Histogram plot of the ^{12}CO excitation temperatures of the potentially triggered (solid line) and the untriggered (dash-dotted line) samples.

We note that, of the 12 potentially triggered BRCs that were observed in CO, nine are associated with non-Gaussian line profiles. Furthermore, two of these (SFO 1 and 2) were not observed in ^{12}CO and so this number may be as high as 90 per cent. Of the ^{12}CO emission profiles of the potentially triggered sample, only the SFO 15 spectrum fails to show any deviation from a Gaussian shape. If, as mentioned earlier, these non-Gaussian profiles are indicative of dynamic activity within these clouds then it is interesting to note the large proportion of potentially triggered clouds that show evidence of this. In contrast, only approximately half of the group II clouds show signs of dynamical activity.

5 SUMMARY AND CONCLUSIONS

We present CO observations towards a sample of 20 northern hemisphere BRCs. These observations were made using the JCMT in the ^{12}CO, ^{13}CO and C^{18}O (J = 2–1) transitions. Due to time and hour angle constraints, only the ^{13}CO transition was observed towards every source, with ^{12}CO and C^{18}O transitions observed towards 17 and 18 clouds, respectively. We find non-Gaussian profiles towards a large portion of the sample (∼65 per cent) which could indicate the presence of dynamical motions within the star-forming cores, such as shocked gas, outflows and infall. Although it is not possible to investigate the nature of these profiles in any depth with single spectra, their presence is consistent with ongoing star formation within a large portion of these clouds. We calculate the internal temperatures of the clouds from the ratio of the moderately optically thick ^{13}CO and optically thin C^{18}O transitions. The external temperatures of the clouds have been calculated from the optically thick ^{12}CO transition. Column densities of the molecular gas associated with these clouds have been determined.

Using a combination of archival radio and mid-IR data, and submm observations, we have refined the SFO catalogue, excluding 18 BRCs that do not show any evidence of photoionization. The remaining 26 clouds that are being photoionized are excellent candidates with which to further investigate the RDI mode of triggered star formation.

Comparing the physical parameters of the triggered and untriggered samples, we find significant differences in the external temperatures of the clouds. We find the surface temperatures of the potentially triggered clouds are significantly higher (by ∼10 K) than those in which triggering is considered unlikely. These higher surface temperatures are the result of external heating by the nearby OB stars which are clearly having a significant impact on the clouds as evinced by the presence of an IBL.

The observations presented here form part of a larger programme designed to investigate the RDI mode of star formation. These single pointing observations are a first step towards studying the molecular gas associated with these triggered star-forming regions. The aim of these observations is to identify kinematic signatures commonly associated with star formation, such as outflow motions and shocked gas. Mapping observations are planned to follow-up the observations presented here, the result of which will be published in a subsequent paper.

ACKNOWLEDGMENTS

The authors would like to thank an anonymous referee for the perceptive comments which have improved the quality of this paper. The authors would also like to thank the Director and staff of the JAC for their hospitality and assistance during our observations. The JCMT is operated by the Joint Astronomy Centre on behalf of the STFC for the United Kingdom, the Netherlands Organisation of Scientific Research and the National Research Council of Canada. We would also like to thank Luke Hindson for his help with ACSIS data reduction and analysis. LKM would like to acknowledge the support of NSERC. JSU is supported by STFC and CSIRO postdoctoral grants. This research would not have been possible without the SIMBAD astronomical data base service operated at CDS, Strasbourg, France and the NASA Astrophysics Data System Bibliographic Services.

REFERENCES

Beltrán M. T., Wiseman J., Ho P. T. P., Estalella R., Fuller G. A., Wootten A., 2008, A&A, 485, 517
Bertoldi F., 1989, ApJ, 346, 735
Chauhan N., Pandey A. K., Ogura K., Ojha D. K., Bhatt B. C., Ghosh S. K., Rawat P. S., 2009, MNRAS, 396, 964
Condon J. J., Cotton W. D., Greisen E. W., Yin Q. F., Perley R. A., Taylor G. B., Broderick J. J., 1998, AJ, 115, 1693
De Vries C. H., Narayanan G., Snell R. L., 2002, ApJ, 577, 798
Elmegreen B. G., Moran J. M., 1979, ApJ, 227, L93
Fukui Y., Iwata T., Mizuno A., Bally J., Lane A. P., 1993, in Levy E. H., Lunine J. I., eds, Protostars and Planets III Molecular outflows. Univ. of Arizona Press, Tucson, p. 603
Getman K. V., Feigelson E. D., Garmire G., Broos P., Wang J., 2007, ApJ, 654, 316
Getman K. V., Feigelson E. D., Luhman K. L., Sicilia-Aguilar A., Wang J., Garmire G. P., 2009, ApJ, 699, 1454
Goldsmith P. F., Bergin E. A., Lis D. C., 1996, in Latter W. B., Radford S. J. E., Jewell P. R., Mangum J. G., Bally J., eds, Proc. IAU Symp. 170, CO: Twenty-Five Years of Millimeter-Wave Spectroscopy. Kluwer Academic Publishers, Dordrecht, p. 113
Gritschneder M., Naab T., Burkert A., Walch S., Heitsch F., Wetzstein M., 2009, MNRAS, 393, 21
Ikeda H. et al., 2008, AJ, 135, 2323
Koenig X. P., Allen L. E., Gutermuth R. A., Hora J. L., Brunt C. M., Muzerolle J., 2008, ApJ, 688, 1142
Kutner M. L., Ulich B. L., 1981, ApJ, 250, 341
Lefloch B., Lazareff B., 1994, A&A, 289, 559
Lefloch B., Lazareff B., Castets A., 1997, A&A, 324, 249
Leger A., Puget J. L., 1984, A&A, 137, L5
Matsuyanagi I., Itoh Y., Sugitani K., Oasa Y., Mukai T., Tamura M., 2006, PASJ, 58, L29
Miao J., White G. J., Nelson R., Thompson M., Morgan L., 2006, MNRAS, 369, 143
Miao J., White G. J., Thompson M. A., Nelson R. P., 2009, ApJ, 692, 382
Morgan L. K., Thompson M. A., Urquhart J. S., White G. J., Miao J., 2004, A&A, 426, 535 (Paper I)
Morgan L. K., Thompson M. A., Urquhart J. S., White G. J., 2008, A&A, 477, 557 (Paper II)
Myers P. C., Mardones D., Tafalla M., Williams J. P., Wilner D. J., 1996, ApJ, 465, L133
Prestage R. M., Meyerdierks H., Lightfoot J. F., Jenness T., Tilanus R. P. J., Padman R., 2000, Starlink User Note 17, http://www.starlink.rl.ac.uk/star/docs/sun17.htx/sun17.html
Reipurth B., 1983, A&A, 117, 183
Savage C., Apponi A. J., Ziurys L. M., Wyckoff S., 2002, ApJ, 578, 211
Sharpless S., 1959, ApJS, 4, 257
Sugitani K., Ogura K., 1994, ApJS, 92, 163
Sugitani K., Fukui Y., Ogura K., 1991, ApJS, 77, 59
Thompson M. A., White G. J., 2004, A&A, 419, 599
Thompson M. A., Urquhart J. S., White G. J., 2004, A&A, 415, 627
Thompson M. A., White G. J., Morgan L. K., Miao J., Fridlund C. V. M., Huldtgren-White M., 2004, A&A, 414, 1017
Urquhart J. S., Thompson M. A., Morgan L. K., White G. J., 2004, A&A, 428, 723
Urquhart J. S., Thompson M. A., Morgan L. K., White G. J., 2006, A&A, 450, 625
Urquhart J. S., Thompson M. A., Morgan L. K., Pestalozzi M. R., White G. J., Muna D. N., 2007, A&A, 467, 1125
Urquhart J. S., Morgan L. K., Thompson M. A., 2009, A&A, 497, 789
White G. J., Lefloch B., Fridlund C. V. M., Aspin C. A., Dahmen G., Minchin N. R., Huldtgren M., 1997, A&A, 323, 931
Wu Y., Wei Y., Zhao M., Shi Y., Yu W., Qin S., Huang M., 2004, A&A, 426, 503

This paper has been typeset from a TEX/LATEX file prepared by the author.